Journal of Computational Physics 358 (2018) 36–52

Contents lists available at ScienceDirect

Journal of Computational Physics

www.elsevier.com/locate/jcp

Well-balanced schemes for the Euler equations with gravitation: Conservative formulation using global fluxes

Alina Chertock [a], Shumo Cui [b], Alexander Kurganov [c,d,*], Şeyma Nur Özcan [a], Eitan Tadmor [e]

[a] Department of Mathematics, North Carolina State University, Raleigh, NC 27695, USA
[b] Department of Mathematics, Temple University, Philadelphia, PA 19122, USA
[c] Department of Mathematics, Southern University of Science and Technology, Shenzhen, 518055, China
[d] Mathematics Department, Tulane University, New Orleans, LA 70118, USA
[e] Department of Mathematics, Center of Scientific Computation and Mathematical Modeling (CSCAMM), Institute for Physical Sciences and Technology (IPST), University of Maryland, College Park, MD 20742, USA

ARTICLE INFO

Article history:
Received 28 July 2017
Received in revised form 7 November 2017
Accepted 19 December 2017
Available online 4 January 2018

Keywords:
Euler equations of gas dynamics with gravitation
Well-balanced scheme
Equilibrium variables
Central-upwind scheme
Piecewise linear reconstruction

ABSTRACT

We develop a second-order well-balanced central-upwind scheme for the compressible Euler equations with gravitational source term. Here, we advocate a new paradigm based on a purely conservative reformulation of the equations using global fluxes. The proposed scheme is capable of exactly preserving steady-state solutions expressed in terms of a nonlocal equilibrium variable. A crucial step in the construction of the second-order scheme is a well-balanced piecewise linear reconstruction of equilibrium variables combined with a well-balanced central-upwind evolution in time, which is adapted to reduce the amount of numerical viscosity when the flow is at (near) steady-state regime. We show the performance of our newly developed central-upwind scheme and demonstrate importance of perfect balance between the fluxes and gravitational forces in a series of one- and two-dimensional examples.

1. Introduction

We are interested in approximations of nonlinear hyperbolic systems of balance laws,

$$\boldsymbol{q}_t + \nabla_{\boldsymbol{x}} \cdot \vec{\boldsymbol{F}}(\boldsymbol{q}) = \boldsymbol{S}(\boldsymbol{q}), \tag{1.1}$$

where $\boldsymbol{x} \in \mathbb{R}^d$ is a multivariate space variable, t is the time, $\vec{\boldsymbol{F}}(\boldsymbol{q})$ is a flux, and $\boldsymbol{S}(\boldsymbol{q})$ is a source term. Our main concern is with *well-balanced* approximations for such systems, which have to address two competing aspects of (1.1). On one hand, they employ conservative discretization of the nonlinear flux to produce high-resolution approximation of the transient solution, $\boldsymbol{q} = \boldsymbol{q}(\boldsymbol{x}, t)$. On the other hand, a well-balanced scheme is expected to capture the correct steady-state solutions, $\boldsymbol{q}_\infty = \boldsymbol{q}_\infty(\boldsymbol{x})$, satisfying $\nabla_{\boldsymbol{x}} \cdot \vec{\boldsymbol{F}}(\boldsymbol{q}_\infty) = \boldsymbol{S}(\boldsymbol{q}_\infty)$.

To make our ideas concrete, we focus on the compressible Euler equations with gravitation, which in the two-dimensional (2-D) case reads as

* Corresponding author.
E-mail addresses: chertock@math.ncsu.edu (A. Chertock), shumo.cui@temple.edu (S. Cui), kurganov@math.tulane.edu (A. Kurganov), snozcan@ncsu.edu (Ş.N. Özcan), tadmor@cscamm.umd.edu (E. Tadmor).

https://doi.org/10.1016/j.jcp.2017.12.026
0021-9991/

$$\begin{cases} \rho_t + (\rho u)_x + (\rho u)_y = 0, \\ (\rho u)_t + (\rho u^2 + p)_x + (\rho uv)_y = -\rho\phi_x, \\ (\rho u)_t + (\rho uv)_x + (\rho v^2 + p)_y = -\rho\phi_y, \\ E_t + (u(E+p)_x + (v(E+p))_y = -\rho u\phi_x - \rho v\phi_y, \end{cases} \tag{1.2}$$

where ρ is the density, u and v are the velocities in the x- and y-directions, respectively, E is the total energy, $p := (\gamma-1)(E - \frac{1}{2}\rho(u^2+v^2))$ is the pressure, and ϕ is the time-independent continuous gravitational potential.

The system of balance laws (1.2) is used to model astrophysical and atmospheric phenomena including supernova explosions [12,13], (solar) climate modeling and weather forecasting [2]. In many physical applications, solutions of this system are sought as small perturbations of the underlying steady states. Capturing such solutions numerically is a challenging task since the size of these perturbations may be smaller than the size of the truncation error affordable by the given computational grid. It is important therefore, to design a *well-balanced* numerical method, which is capable of exactly preserving (certain) steady-state solutions, so that the perturbed solutions will be resolved on the given grid, free of non-physical spurious oscillations.

1.1. Conservative formulation using global fluxes

Well-balanced schemes were introduced in [10] and mainly developed in the context of shallow water equations; see, e.g., [1,4,6,7,11,16,19,25–27,33] and references therein. Further extensions to Euler equations with gravitation will be mentioned below. Here, we advocate a new approach for designing well-balanced schemes for the system (1.2). Our starting point is to rewrite this system by incorporating the gravitational source terms into the corresponding momentum and energy fluxes, thus arriving at the following *purely conservative formulation*:

$$\begin{cases} \rho_t + (\rho u)_x + (\rho v)_y = 0, \\ (\rho u)_t + (\rho u + K)_x + (\rho uv)_y = 0, \\ (\rho v)_t + (\rho uv)_x + (\rho v^2 + L)_y = 0, \\ (E + \rho\phi)_t + (u(E + \rho\phi + p))_x + (v(E + \rho\phi + p))_y = 0. \end{cases} \tag{1.3}$$

Here, $K := p + Q$ and $L := p + R$, where Q and R involve the *global variables*

$$Q(x,y,t) := \int^x \rho(\xi,y,t)\phi_x(\xi,y)\,d\xi, \quad R(x,y,t) := \int^y \rho(x,\eta,t)\phi_y(x,\eta)\,d\eta. \tag{1.4}$$

It is the global momentum fluxes in (1.3), (1.4) that play a central role in our proposed approach. We argue below, both theoretically and demonstrate numerically, that the use of such purely conservative formulation (1.3), (1.4) is an effective approach to capture arbitrary (without any assumption of a thermal equilibrium) motionless steady states given by

$$u \equiv 0, \quad v \equiv 0, \quad K_x \equiv 0, \quad L_y \equiv 0. \tag{1.5}$$

To this end, one needs to carefully integrate the global variables Q and R on the fly, to recover the reformulated momentum equations in terms of the corresponding global fluxes on the left-hand side of the second and third equations in (1.3). The use of such global fluxes is not easily amenable, however, for numerical approximations which make use of (approximate) Riemann problem solvers. Instead, our well-balanced approach employs the class of *central-upwind* (CU) schemes, [14,15,17,18], which offer highly accurate Godunov-type finite-volume methods that do *not* require any (approximate) Riemann problem solver, and as such are natural candidates for numerical approximation of global-flux based formulation of the Euler equations (1.3). The adaptation of the CU schemes in the present context of global flux must be handled with care: in §2.1 we show that a high-order reconstruction of the *conservative* variables $(\rho, \rho u, \rho v, E)^\top$ do not possess the well-balanced property. Instead, we introduce a special reconstruction based on the *equilibrium variables*, $(\rho, \rho u, \rho v, K, L)^\top$ rather than the conservative ones. The resulting well-balanced CU schemes in the one- and two-dimensional cases are developed in §2 and §3, respectively. In §4, we present a series of examples of one- and two-dimensional numerical simulations which confirm the desired performance of our proposed well-balanced, high-resolution CU scheme is coupled with the global-based fluxes of purely conservative formulation.

We close this introduction with a brief overview of related work on well-balanced schemes for the Euler equations with gravitational fields. In [20], quasi-steady wave-propagation methods were developed for models with a static gravitational field. In [2], well-balanced finite-volume methods, which preserve a certain class of steady states, were derived for nearly hydrostatic flows. The recent works [3,5,13,31] introduce finite-volume methods with carefully reconstructed solutions that handle more general gravitational potentials and preserve more general classes of steady states. In [23,30,34], gas-kinetic schemes were extended to the multidimensional gas dynamic equations and well-balanced numerical methods were developed for problems, in which the gravitational potential was modeled by a piecewise step function. More recently, higher order finite-difference [32] and finite-volume [21] methods for the gas dynamics with gravitation have been introduced.

In summary, we advocate the three main ingredients of the proposed approach: (i) the reformulation of Euler systems with gravitational source field as a purely conservative system using global-based fluxes; (ii) the use of Riemann-problem-solver free CU schemes to advance a highly-accurate numerical solution for such systems; and (iii) the reconstruction of such numerical solution using equilibrium rather conservative variables.

2. One-dimensional central-upwind scheme

In this section, we briefly describe the semi-discrete CU scheme applied to the one-dimensional (1-D) version of the system (1.3) considered in the y-direction:

$$\boldsymbol{q}_t + \boldsymbol{G}(\boldsymbol{q})_y = \boldsymbol{0}, \tag{2.1}$$

where

$$\boldsymbol{q} = (\rho, \rho v, E + \rho\phi)^\top, \quad \boldsymbol{G}(\boldsymbol{q}) = \Big(\rho v, \rho v^2 + L, v(E + \rho\phi + p)\Big)^\top \tag{2.2}$$

and

$$p = (\gamma - 1)\Big(E - \frac{1}{2}\rho v^2\Big). \tag{2.3}$$

The simplest steady state of (2.1)–(2.3) is the motionless one for which

$$v \equiv 0, \quad L \equiv \text{Const}. \tag{2.4}$$

We assume that the cell averages of the numerical solution, $\overline{\boldsymbol{q}}_k(t) := \frac{1}{\Delta y}\int_{C_k} \boldsymbol{q}(y,t)\,dy$, are available at time t. Here, $\{C_k\}$ is a partition of the computational domain into finite-volume cells $C_k := [y_{k-\frac{1}{2}}, y_{k+\frac{1}{2}}]$ of size $|C_k| = \Delta y$ centered at y_k, $k = k_\ell, \ldots, k_r$. To advance the solution in time, we use the semi-discrete CU scheme [14] applied to (2.1)–(2.3) which results in the following system of ODEs:

$$\frac{d}{dt}\overline{\boldsymbol{q}}_k = -\frac{\mathcal{G}_{k+\frac{1}{2}} - \mathcal{G}_{k-\frac{1}{2}}}{\Delta y}, \tag{2.5}$$

computed in terms of the CU numerical flux

$$\mathcal{G}_{k+\frac{1}{2}} := \frac{b^+_{k+\frac{1}{2}}\boldsymbol{G}(\boldsymbol{q}^{\mathrm{N}}_k) - b^-_{k+\frac{1}{2}}\boldsymbol{G}(\boldsymbol{q}^{\mathrm{S}}_{k+1})}{b^+_{k+\frac{1}{2}} - b^-_{k+\frac{1}{2}}} + \beta_{k+\frac{1}{2}}\Big(\boldsymbol{q}^{\mathrm{S}}_{k+1} - \boldsymbol{q}^{\mathrm{N}}_k - \delta\boldsymbol{q}_{k+\frac{1}{2}}\Big), \quad \beta_{k+\frac{1}{2}} := \frac{b^+_{k+\frac{1}{2}}b^-_{k+\frac{1}{2}}}{b^+_{k+\frac{1}{2}} - b^-_{k+\frac{1}{2}}}. \tag{2.6}$$

Here,

$$\boldsymbol{q}^{\mathrm{N}}_k := \widetilde{\boldsymbol{q}}(y_{k+\frac{1}{2}} - 0) = \overline{\boldsymbol{q}}_k + \frac{\Delta y}{2}(\boldsymbol{q}_y)_k \quad \text{and} \quad \boldsymbol{q}^{\mathrm{S}}_{k+1} := \widetilde{\boldsymbol{q}}(y_{k+\frac{1}{2}} + 0) = \overline{\boldsymbol{q}}_{k+1} - \frac{\Delta y}{2}(\boldsymbol{q}_y)_{k+1} \tag{2.7}$$

are the one-sided point values of the computed solution at the "North" and "South" cell interfaces $y = y_{k+\frac{1}{2}}$, which are recovered from a second-order piecewise linear reconstruction

$$\widetilde{\boldsymbol{q}}(y) = \sum_k \big(\overline{\boldsymbol{q}}_k + (\boldsymbol{q}_y)_k(y - y_k)\big)\chi_{C_k}(y), \quad \chi_{C_k}(y) = \begin{cases} 1, \text{ if } y \in C_k, \\ 0, \text{ otherwise.} \end{cases}$$

To avoid oscillations, the vertical slopes in (2.7), $(\boldsymbol{q}_y)$, are to be computed with the help a nonlinear limiter. In our numerical experiments reported below, we have used the generalized minmod limiter applied component-wise; see, e.g., [22,24,29]:

$$(\boldsymbol{q}_y)_k = \text{minmod}\left(\theta\,\frac{\overline{\boldsymbol{q}}_{k+1} - \overline{\boldsymbol{q}}_k}{\Delta y}, \frac{\overline{\boldsymbol{q}}_{k+1} - \overline{\boldsymbol{q}}_{k-1}}{2\Delta y}, \theta\,\frac{\overline{\boldsymbol{q}}_k - \overline{\boldsymbol{q}}_{k-1}}{\Delta y}\right).$$

The parameter $\theta \in [1, 2]$ controls the amount of numerical dissipation: larger values of θ typically lead to less dissipative but more oscillatory scheme.

Equipped with the reconstructed point values $\boldsymbol{q}^{\mathrm{N,S}}_k = \big(\rho^{\mathrm{N,S}}_k, (\rho v)^{\mathrm{N,S}}_k, (E + \rho\phi)^{\mathrm{N,S}}_k\big)^\top$, we obtain the point values of the other variables needed in the computation of the numerical fluxes in (2.6), that is,

$$v^{\mathrm{N,S}}_k = \frac{(\rho v)^{\mathrm{N,S}}_k}{\rho^{\mathrm{N,S}}_k}, \quad p^{\mathrm{N,S}}_k = (\gamma - 1)\left[(E + \rho\phi)^{\mathrm{N,S}}_k - (\rho\phi)^{\mathrm{N,S}}_k - \frac{\rho^{\mathrm{N,S}}_k (v^{\mathrm{N,S}}_k)^2}{2}\right],$$

and

$$L^{\rm N}_k = p^{\rm N}_k + R_{k+\frac12}, \quad L^{\rm S}_k = p^{\rm S}_k + R_{k-\frac12},$$

where $\{R_{k+\frac12}\}$ are calculated recursively using the midpoint quadrature rule:

$$R_{k_\ell-\frac12} = 0, \qquad R_{k+\frac12} = R_{k-\frac12} + \Delta y\,\overline{\rho}_k(\phi_y)_k, \qquad k = k_\ell,\ldots,k_r, \tag{2.8}$$

and $(\rho\phi)^{\rm N}_k = \rho^{\rm N}_k\phi(y_{k+\frac12})$, $(\rho\phi)^{\rm S}_k = \rho^{\rm S}_k\phi(y_{k-\frac12})$, and $(\phi_y)_k := \phi_y(y_k)$.

The terms $b^{\pm}_{k+\frac12}$ are one-sided local speeds of propagation, which can be estimated using the smallest and largest eigenvalues of the Jacobian $\partial\boldsymbol{G}/\partial\boldsymbol{q}$:

$$b^+_{k+\frac12} = \max\Big(v^{\rm N}_k + c^{\rm N}_k,\ v^{\rm S}_{k+1} + c^{\rm S}_{k+1},\ 0\Big), \quad b^-_{k+\frac12} = \min\Big(v^{\rm N}_k - c^{\rm N}_k,\ v^{\rm S}_{k+1} - c^{\rm S}_{k+1},\ 0\Big), \tag{2.9}$$

where $c^{\rm N,S}_{k+1}$ are the speeds of sound ($c^2 = \gamma p/\rho$).

Finally, the second term on the right-hand side (RHS) of (2.6) is a built-in *anti-diffusion term* which involves $\delta\boldsymbol{q}_{k+\frac12} = \text{minmod}\big(\boldsymbol{q}^{\rm S}_{k+1} - \boldsymbol{q}^*_{k+\frac12},\ \boldsymbol{q}^*_{k+\frac12} - \boldsymbol{q}^{\rm N}_k\big)$ using the intermediate state

$$\boldsymbol{q}^*_{k+\frac12} = \frac{b^+_{k+\frac12}\boldsymbol{q}^{\rm S}_{k+1} - b^-_{k+\frac12}\boldsymbol{q}^{\rm N}_k - \big(\boldsymbol{G}(\boldsymbol{q}^{\rm S}_{k+1}) - \boldsymbol{G}(\boldsymbol{q}^{\rm N}_k)\big)}{b^+_{k+\frac12} - b^-_{k+\frac12}}. \tag{2.10}$$

2.1. Lack of well-balancing

The CU scheme (2.5)–(2.10) is not capable of exactly preserving the steady-state solution (2.4). Indeed, substituting $v \equiv 0$ into (2.5)–(2.10) and noting that for all k, $b^+_{k+\frac12} = -b^-_{k+\frac12}$ (since $v^{\rm N}_k = v^{\rm S}_{k+1} = 0$), we obtain the ODE system

$$\begin{cases} \dfrac{d\overline{\rho}_k}{dt} = -\dfrac{1}{\Delta y}\Big[\beta_{k+\frac12}(\rho^{\rm S}_{k+1} - \rho^{\rm N}_k - \delta\rho_{k+\frac12}) - \beta_{k-\frac12}(\rho^{\rm S}_k - \rho^{\rm N}_{k-1} - \delta\rho_{k-\frac12})\Big], \\ \dfrac{d(\overline{\rho v})_k}{dt} = -\dfrac{1}{2\Delta y}\Big[(L^{\rm S}_{k+1} + L^{\rm N}_k) - (L^{\rm S}_k + L^{\rm N}_{k-1})\Big], \\ \dfrac{d(\overline{E}_k + \overline{\rho}_k\phi_k)}{dt} = -\dfrac{1}{\Delta y}\Big[\beta_{k+\frac12}(E+\rho\phi)^{\rm S}_{k+1} - (E+\rho\phi)^{\rm N}_k - \delta(E+\rho\phi)_{k+\frac12} \\ \qquad\qquad -\beta_{k-\frac12}((E+\rho\phi)^{\rm S}_k - (E+\rho\phi)^{\rm N}_{k-1} - \delta(E+\rho\phi)_{k-\frac12}\Big], \end{cases} \tag{2.11}$$

whose RHS does not necessarily vanish and hence the steady state (2.4) would not be preserved at the discrete level. We would like to stress that even for the first-order version of the CU scheme (2.5)–(2.10), that is, when $(\boldsymbol{q}_y)_k \equiv 0$ in (2.7), the RHS of (2.11) does not vanish. This means that the lack of balance between the numerical flux and source terms is a fundamental problem of the scheme. We also note that for smooth solutions, the balance error in (2.11) is expected to be of order $(\Delta y)^2$, but a coarse grid solution may contain large spurious waves as demonstrated in the numerical experiments presented in §4.

2.2. Well-balanced central-upwind scheme

In this section, we present a well-balanced modification of the CU scheme. We first introduce a *well-balanced reconstruction*, which is performed on the equilibrium variables rather than the conservative ones, and then apply a slightly modified CU scheme to the system (2.1)–(2.3).

Well-balanced reconstruction. We now describe a special reconstruction, which is used in the derivation of a well-balanced CU scheme. The main idea is to reconstruct equilibrium variable L rather than E. For the first two components we still use the same piecewise linear reconstructions as before, $\widetilde{\rho}(y)$ and $(\widetilde{\rho v})(y)$, and compute the corresponding point values of $\rho^{\rm N,S}_k$, $(\rho v)^{\rm N,S}_k$, and $v^{\rm N,S}_k$.

In order to reconstruct $L = p + R$, we use the cell-interface point values $R_{k\pm\frac12}$ in (2.8) and compute the corresponding values of R at the cell centers as

$$R_k = \frac12\Big(R_{k-\frac12} + R_{k+\frac12}\Big), \qquad k = k_\ell,\ldots,k_r, \tag{2.12}$$

and thus the values of L at the cell centers are

$$L_k = p_k + R_k, \tag{2.13}$$

where $p_k=(\gamma-1)\left(\overline{E}_k-\frac{\overline{\rho}_k}{2}v_k^2\right)$ is obtained from the corresponding equation of state (EOS) and $v_k=(\overline{\rho v})_k/\overline{\rho}_k$. Equipped with (2.13), we then apply the minmod reconstruction procedure to $\{L_k\}$ and obtain the point values of L at the cell interfaces:

$$L_k^{\rm N}=L_k+\frac{\Delta y}{2}(L_y)_k,\quad L_{k+1}^{\rm S}=L_{k+1}-\frac{\Delta y}{2}(L_y)_{k+1},$$

where the slopes $\{(L_y)_k\}$ are computed using the generalized minmod limiter. Finally, the point values of p and E needed for computation of numerical fluxes are given by $p_k^{\rm N,S}=L_k^{\rm N,S}-R_{k\pm\frac12}$ and $E_k^{\rm N,S}=\frac{1}{\gamma-1}\,p_k^{\rm N,S}+\frac12\rho_k^{\rm N,S}(v_k^{\rm N,S})^2$, respectively.

Remark 2.1. If the gravitational potential is linear ($\phi(y)=gy$ with g being the gravitational constant), then R can be computed by integrating the piecewise linear reconstruction of ρ, (3.1), which results in the piecewise quadratic approximation of R:

$$\widetilde{R}(y)=g\int\limits_{y_{k_\ell-\frac12}}^{y}\widetilde{\rho}(\xi)\,d\xi=g\sum_k\left[\Delta y\sum_{i=k_\ell}^{k-1}\overline{\rho}_i+\overline{\rho}_k(y-y_{k-\frac12})+\frac{(\rho_y)_k}{2}(y-y_{k-\frac12})(y-y_{k+\frac12})\right]\chi_{C_k}(y).$$

Then, the point values of R at the cell interfaces and at cell centers are given, respectively, by

$$R_{k+\frac12}=g\Delta y\sum_{i=k_\ell}^{k}\overline{\rho}_i\quad\text{and}\quad R_k=g\Delta y\sum_{i=k_\ell}^{k-1}\overline{\rho}_i+\frac{g\Delta y}{2}\,\overline{\rho}_k-\frac{g(\Delta y)^2}{8}(\rho_y)_k.$$

Well-balanced evolution. The cell-averages $\overline{\boldsymbol{q}}_k$ are evolved in time according to the system of ODEs (2.5). The second component of the numerical fluxes $\boldsymbol{\mathcal{G}}$ is computed the same way as in (2.6), but with $\boldsymbol{G}$ given by (2.1)–(2.3), that is,

$$\begin{aligned}\mathcal{G}^{(2)}_{k+\frac12}&=\frac{b^+_{k+\frac12}\left(\rho_k^{\rm N}(v_k^{\rm N})^2+L_k^{\rm N}\right)-b^-_{k+\frac12}\left(\rho_{k+1}^{\rm S}(v_{k+1}^{\rm S})^2+L_{k+1}^{\rm S}\right)}{b^+_{k+\frac12}-b^-_{k+\frac12}}\\&\quad+\beta_{k+\frac12}\left((\rho v)_{k+1}^{\rm S}-(\rho v)_k^{\rm N}-\delta(\rho v)_{k+\frac12}\right),\end{aligned}\tag{2.14}$$

while the first and third components are modified in order to exactly preserve the steady state:

$$\begin{aligned}\mathcal{G}^{(1)}_{k+\frac12}&=\frac{b^+_{k+\frac12}(\rho v)_k^{\rm N}-b^-_{k+\frac12}(\rho v)_{k+1}^{\rm S}}{b^+_{k+\frac12}-b^-_{k+\frac12}}+\beta_{k+\frac12}H(\psi_{k+\frac12})\cdot\left(\rho_{k+1}^{\rm S}-\rho_k^{\rm N}-\delta\rho_{k+\frac12}\right),\\\mathcal{G}^{(3)}_{k+\frac12}&=\frac{b^+_{k+\frac12}v_k^{\rm N}(E_k^{\rm N}+(\rho\phi)_k^{\rm N}+p_k^{\rm N})-b^-_{k+\frac12}v_{k+1}^{\rm S}(E_{k+1}^{\rm S}+(\rho\phi)_{k+1}^{\rm S}+p_{k+1}^{\rm S})}{b^+_{k+\frac12}-b^-_{k+\frac12}}\\&\quad+\beta_{k+\frac12}\left[E_{k+1}^{\rm S}-E_k^{\rm N}+H(\psi_{k+\frac12})\cdot\left((\rho\phi)_{k+1}^{\rm S}-(\rho\phi)_k^{\rm N}-\delta(E+\rho\phi)_{k+\frac12}\right)\right],\end{aligned}\tag{2.15}$$

where $\psi_{k+\frac12}=\frac{|L_{k+1}-L_k|}{\Delta y}\cdot\frac{y_{k_r+\frac12}-y_{k_\ell-\frac12}}{\max\{L_k,L_{k+1}\}}$.

Notice that the last terms on the RHS of (2.15) include a slight modification of the original CU flux, which is now multiplied by a smooth cut-off function H, which is small when the computed solution is locally (almost) at a steady state, where $|L_{k+1}-L_k|/\Delta y\sim0$, and is otherwise close to 1. This is done in order to guarantee the well-balanced property of the scheme, shown in Theorem 2.1 below. A sketch of a typical function H is shown in Fig. 2.1. In all of our numerical experiments, we have used

$$H(\psi)=\frac{(C\psi)^m}{1+(C\psi)^m},\tag{2.16}$$

with $C=200$ and $m=6$. To reduce the dependence of the computed solution on the choice of particular values of C and m, the argument of H in (2.15) is normalized by a factor $\frac{y_{k_r+\frac12}-y_{k_\ell-\frac12}}{\max\{L_k,L_{k+1}\}}$, which makes $H(\psi_{k+\frac12})$ dimensionless.

Theorem 2.1. *The semi-discrete CU scheme (2.5), (2.14), (2.15) coupled with the reconstruction described in §2.2 is well-balanced in the sense that it exactly preserves the steady state (2.4).*

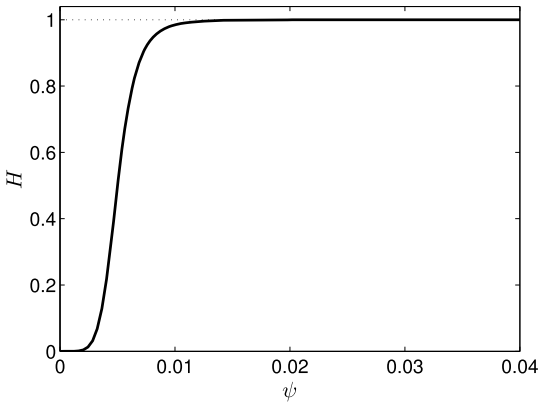

Fig. 2.1. Sketch of $H(\psi)$.

Proof. Assume that at certain time level, we have

$$v_k^{\mathrm{N}} \equiv v_k \equiv v_k^{\mathrm{S}} \equiv 0 \quad \text{and} \quad L_k^{\mathrm{N}} \equiv L_k \equiv L_k^{\mathrm{S}} \equiv \widehat{L}, \tag{2.17}$$

where $\widehat{L}$ is a constant. In order to prove that the proposed scheme is well-balanced, we will show that the numerical fluxes are constant for all k for the data in (2.17) and thus need the RHS of (2.5) is identically equal to zero at such steady states.

Indeed, the first component in (2.15) of the numerical flux vanish since $v_k^{\mathrm{N}} = v_{k+1}^{\mathrm{S}} = 0$ and $L_k = L_{k+1} = \widehat{L}$ (the latter implies $H(\psi_{k+\frac{1}{2}}) = H(0) = 0$). The second component (2.14) of the numerical flux is constant and equal to $\widehat{L}$ since $v_k^{\mathrm{N}} = v_{k+1}^{\mathrm{S}} = 0$ and $L_k^{\mathrm{N}} = L_{k+1}^{\mathrm{S}} = \widehat{L}$. Finally, the third component in (2.15) of the numerical flux also vanishes:

$$\begin{aligned}\mathcal{G}^{(3)}_{k+\frac{1}{2}} &= \beta_{k+\frac{1}{2}}\left[E^{\mathrm{S}}_{k+1} - E^{\mathrm{N}}_k + H(\psi_{k+\frac{1}{2}})\cdot\Big((\rho\phi)^{\mathrm{S}}_{k+1} - (\rho\phi)^{\mathrm{N}}_k - \delta(E+\rho\phi)_{k+\frac{1}{2}}\Big)\right]\\ &= \frac{\beta_{k+\frac{1}{2}}}{\gamma-1}\cdot\frac{p^{\mathrm{S}}_{k+1} - p^{\mathrm{N}}_k}{2} = \frac{\beta_{k+\frac{1}{2}}}{2(\gamma-1)}\left[\big(L^{\mathrm{S}}_{k+1} - R_{k+\frac{1}{2}}\big) - \big(L^{\mathrm{N}}_k - R_{k+\frac{1}{2}}\big)\right] = 0,\end{aligned}$$

since $L_k^{\mathrm{N}} = L_{k+1}^{\mathrm{S}} = \widehat{L}$. □

3. Two-dimensional well-balanced central-upwind scheme

In this section, we describe the well-balanced semi-discrete CU scheme for the 2-D Euler equations with gravitation (1.3), which can be rewritten in the following vector form:

$$\boldsymbol{q}_t + \boldsymbol{F}(\boldsymbol{q})_x + \boldsymbol{G}(\boldsymbol{q})_y = \boldsymbol{0},$$

where $\boldsymbol{q} := (\rho, \rho u, \rho v, E + \rho\phi)^\top$, the fluxes are

$$\boldsymbol{F}(\boldsymbol{q}) := (\rho u, \rho u^2 + K, \rho uv, u(E + \rho\phi + p))^\top, \quad \boldsymbol{G}(\boldsymbol{q}) := (\rho v, \rho uv, \rho v^2 + L, v(E + \rho\phi + p))^\top,$$

in which $K = p + Q$ and $L = p + R$ with the global variables Q and R introduced in (1.4).

Let $C_{j,k} := [x_{j-\frac{1}{2}}, x_{j+\frac{1}{2}}] \times [y_{k-\frac{1}{2}}, y_{k+\frac{1}{2}}]$ denote the 2-D cells and we assume that the cell averages of the computed numerical solution,

$$\overline{\boldsymbol{q}}_{j,k}(t) := \frac{1}{\Delta x\Delta y}\iint\limits_{C_{j,k}} \boldsymbol{q}(x,y,t)\,dx\,dy, \qquad j = j_\ell, \ldots, j_r,\ k = k_\ell, \ldots, k_r$$

are available at time level t and describe their CU evolution.

Well-balanced reconstruction. Similarly to the 1-D case, we reconstruct only the first three components of the conservative variables, $\rho, \rho u, \rho v$,

$$\widetilde{q}^{\,(i)}(x,y) = \overline{q}^{\,(i)}_{j,k} + (q^{(i)}_x)_{j,k}(x - x_j) + (q^{(i)}_y)_{j,k}(y - y_k), \quad (x,y) \in C_{j,k},\ \ i = 1,2,3, \tag{3.1}$$

and obtain the corresponding point values at the four cell interfaces $(x_{j\pm\frac{1}{2}}, y_k)$ and $(x_j, y_{k\pm\frac{1}{2}})$ denoted $(q^{(i)})^{\mathrm{E,W,N,S}}_{j,k}$ with the slopes $(q^{(i)}_x)_{j,k}$ and $(q^{(i)}_y)_{j,k}$ being computed using the generalized minmod limiter.

The point values of the energy p and E should be calculated from the new equilibrium variables obtained from the reconstruction of K and L. We emphasize that since at the steady states (1.5), $K = K(y)$ is independent of x and $L = L(x)$ is independent of y, we, in fact, perform 1-D reconstructions for K and L in the x- and y-directions, respectively. To this end, we first use the midpoint rule to compute the point values of the integrals Q and R in (1.4) at the cell interfaces in the x- and y-directions, respectively:

$$\begin{aligned}
&Q_{j_\ell-\frac{1}{2},k}=0,\quad \begin{cases} Q_{j+\frac{1}{2},k}=Q_{j-\frac{1}{2},k}+\Delta x\overline{\rho}_{j,k}(\phi_x)_{j,k},\\ Q_{j,k}=\dfrac{1}{2}\left\{Q_{j-\frac{1}{2},k}+Q_{j+\frac{1}{2},k}\right\}, \end{cases} \quad j=j_\ell,\ldots,j_r,\ k=k_\ell,\ldots,k_r,\\
&R_{j,k_\ell-\frac{1}{2}}=0,\quad \begin{cases} R_{j,k+\frac{1}{2}}=R_{j,k-\frac{1}{2}}+\Delta y\,\overline{\rho}_{j,k}(\phi_y)_{j,k},\\ R_{j,k}=\dfrac{1}{2}\left\{R_{j,k-\frac{1}{2}}+R_{j,k+\frac{1}{2}}\right\}, \end{cases} \quad j=j_\ell,\ldots,j_r,\ k=k_\ell,\ldots,k_r,
\end{aligned} \tag{3.2}$$

where $(\phi_x)_{j,k}:=\phi_x(x_j,y_k)$ and $(\phi_y)_{j,k}:=\phi_y(x_j,y_k)$. We then compute the cell center values $K_{j,k}=p_{j,k}+Q_{j,k}$ and $L_{j,k}=p_{j,k}+R_{j,k}$, and reconstruct the point values of K and L at the cell interfaces,

$$\begin{aligned}
&K^{\rm E}_{j,k}=K_{j,k}+\frac{\Delta x}{2}(K_x)_{j,k},K^{\rm W}_{j,k}=K_{j,k}-\frac{\Delta x}{2}(K_x)_{j,k},\\
&L^{\rm N}_{j,k}=L_{j,k}+\frac{\Delta y}{2}(L_y)_{j,k},\ L^{\rm S}_{j,k}=L_{j,k}-\frac{\Delta y}{2}(L_y)_{j,k},
\end{aligned} \tag{3.3}$$

where $(K_x)_{j,k}$ and $(L_y)_{j,k}$ are the minmod limited slopes in the x- and y- directions, respectively. Finally, the values obtained in (3.3) are used to evaluate the point values of the pressure

$$\begin{aligned}
&p^{\rm E}_{j,k}=K^{\rm E}_{j,k}-Q_{j+\frac{1}{2},k},p^{\rm W}_{j,k}=K^{\rm W}_{j,k}-Q_{j-\frac{1}{2},k},\\
&p^{\rm N}_{j,k}=L^{\rm N}_{j,k}-R_{j,k+\frac{1}{2}},\ p^{\rm S}_{j,k}=L^{\rm S}_{j,k}-R_{j,k-\frac{1}{2}},
\end{aligned}$$

and then the corresponding point values of E are calculated from the EOS, $E=\frac{p}{\gamma-1}+\frac{1}{2}\rho(u^2+v^2)$.

We then estimate the one-sided local speeds of propagation in the x- and y- directions, respectively, using the smallest and largest eigenvalues of the Jacobians $\partial\boldsymbol{F}/\partial\boldsymbol{q}$ and $\partial\boldsymbol{G}/\partial\boldsymbol{q}$:

$$\begin{aligned}
&a^+_{j+\frac{1}{2},k}=\max\left(u^{\rm E}_{j,k}+c^{\rm E}_{j,k},\,u^{\rm W}_{j+1,k}+c^{\rm W}_{j+1,k},\,0\right),\quad a^-_{j+\frac{1}{2},k}=\min\left(u^{\rm E}_{j,k}-c^{\rm E}_{j,k},\,u^{\rm W}_{j+1,k}-c^{\rm W}_{j+1,k},\,0\right),\\
&b^+_{j,k+\frac{1}{2}}=\max\left(v^{\rm N}_{j,k}+c^{\rm N}_{j,k},\,v^{\rm S}_{j,k+1}+c^{\rm S}_{j,k+1},\,0\right),\quad b^-_{j,k+\frac{1}{2}}=\min\left(v^{\rm N}_{j,k}-c^{\rm N}_{j,k},\,v^{\rm S}_{j,k+1}-c^{\rm S}_{j,k+1},\,0\right),
\end{aligned}$$

in terms of the velocities, $u^{\rm E,W,N,S}_{j,k}$, and the speeds of sound, $c^{\rm E,W,N,S}_{j,k}$.

Well-balanced evolution. The cell-averages $\overline{\boldsymbol{q}}$ are evolved in time according to the following system of ODEs:

$$\frac{d}{dt}\overline{\boldsymbol{q}}_{j,k}=-\frac{\boldsymbol{\mathcal{F}}_{j+\frac{1}{2},k}-\boldsymbol{\mathcal{F}}_{j-\frac{1}{2},k}}{\Delta x}-\frac{\boldsymbol{\mathcal{G}}_{j,k+\frac{1}{2}}-\boldsymbol{\mathcal{G}}_{j,k-\frac{1}{2}}}{\Delta y}, \tag{3.4}$$

where $\boldsymbol{\mathcal{F}}$ and $\boldsymbol{\mathcal{G}}$ are numerical fluxes. Introducing the notations

$$\alpha_{j+\frac{1}{2},k}:=\frac{a^+_{j+\frac{1}{2},k}a^-_{j+\frac{1}{2},k}}{a^+_{j+\frac{1}{2},k}-a^-_{j+\frac{1}{2},k}}\quad\text{and}\quad\beta_{j,k+\frac{1}{2}}:=\frac{b^+_{j,k+\frac{1}{2}}b^-_{j,k+\frac{1}{2}}}{b^+_{j,k+\frac{1}{2}}-b^-_{j,k+\frac{1}{2}}},$$

we write the components of $\boldsymbol{\mathcal{F}}_{j+\frac{1}{2},k}$ and $\boldsymbol{\mathcal{G}}_{j,k+\frac{1}{2}}$ as

$$\begin{aligned}
\mathcal{F}^{(1)}_{j+\frac{1}{2},k}&=\frac{a^+_{j+\frac{1}{2},k}(\rho u)^{\rm E}_{j,k}-a^-_{j+\frac{1}{2},k}(\rho u)^{\rm W}_{j+1,k}}{a^+_{j+\frac{1}{2},k}-a^-_{j+\frac{1}{2},k}}+\alpha_{j+\frac{1}{2},k}H(\psi_{j+\frac{1}{2},k})\cdot\left(\rho^{\rm W}_{j+1,k}-\rho^{\rm E}_{j,k}-\delta\rho_{j+\frac{1}{2},k}\right),\\
\mathcal{F}^{(2)}_{j+\frac{1}{2},k}&=\frac{a^+_{j+\frac{1}{2},k}\left(\rho^{\rm E}_{j,k}(u^{\rm E}_{j,k})^2+K^{\rm E}_{j,k}\right)-a^-_{j+\frac{1}{2},k}(\rho^{\rm W}_{j+1,k}(u^{\rm W}_{j+1,k})^2+K^{\rm W}_{j+1,k})}{a^+_{j+\frac{1}{2},k}-a^-_{j+\frac{1}{2},k}}\\
&\quad+\alpha_{j+\frac{1}{2},k}\left((\rho u)^{\rm W}_{j+1,k}-(\rho u)^{\rm E}_{j,k}-\delta(\rho u)_{j+\frac{1}{2},k}\right),
\end{aligned}$$

$$\mathcal{F}^{(3)}_{j+\frac12,k}=\frac{a^+_{j+\frac12,k}\rho^{\rm E}_{j,k}u^{\rm E}_{j,k}v^{\rm E}_{j,k}-a^-_{j+\frac12,k}\rho^{\rm W}_{j+1,k}u^{\rm W}_{j+1,k}v^{\rm W}_{j+1,k}}{a^+_{j+\frac12,k}-a^-_{j+\frac12,k}}+\alpha_{j+\frac12,k}\big((\rho v)^{\rm W}_{j+1,k}-(\rho v)^{\rm E}_{j,k}-\delta(\rho v)_{j+\frac12,k}\big),$$

$$\mathcal{F}^{(4)}_{j+\frac12,k}=\frac{a^+_{j+\frac12,k}u^{\rm E}_{j,k}(E^{\rm E}_{j,k}+(\rho\phi)^{\rm E}_{j,k}+p^{\rm E}_{j,k})-a^-_{j+\frac12,k}u^{\rm W}_{j+1,k}(E^{\rm W}_{j+1,k}+(\rho\phi)^{\rm W}_{j+1,k}+p^{\rm W}_{j+1,k})}{a^+_{j+\frac12,k}-a^-_{j+\frac12,k}}$$
$$+\alpha_{j+\frac12,k}\Big[E^{\rm W}_{j+1,k}-E^{\rm E}_{j,k}+H(\psi_{j+\frac12,k})\cdot\big((\rho\phi)^{\rm W}_{j+1,k}-(\rho\phi)^{\rm E}_{j,k}-\delta(E+\rho\phi)_{j+\frac12,k}\big)\Big],$$

$$\mathcal{G}^{(1)}_{j,k+\frac12}=\frac{b^+_{j,k+\frac12}(\rho v)^{\rm N}_{j,k}-b^-_{j,k+\frac12}(\rho v)^{\rm S}_{j,k+1}}{b^+_{j,k+\frac12}-b^-_{j,k+\frac12}}+\beta_{j,k+\frac12}H(\psi_{j,k+\frac12})\cdot\big(\rho^{\rm S}_{j,k+1}-\rho^{\rm N}_{j,k}-\delta\rho_{j,k+\frac12}\big),$$

$$\mathcal{G}^{(2)}_{j,k+\frac12}=\frac{b^+_{j,k+\frac12}\rho^{\rm N}_{j,k}u^{\rm N}_{j,k}v^{\rm N}_{j,k}-b^-_{j,k+\frac12}\rho^{\rm S}_{j,k+1}u^{\rm S}_{j,k+1}v^{\rm S}_{j,k+1}}{b^+_{j,k+\frac12}-b^-_{j,k+\frac12}}+\beta_{j,k+\frac12}\big((\rho u)^{\rm S}_{j,k+1}-(\rho u)^{\rm N}_{j,k}-\delta(\rho u)_{j,k+\frac12}\big),$$

$$\mathcal{G}^{(3)}_{j,k+\frac12}=\frac{b^+_{j,k+\frac12}\left(\rho^{\rm N}_{j,k}(v^{\rm N}_{j,k})^2+L^{\rm N}_{j,k}\right)-b^-_{j,k+\frac12}\left(\rho^{\rm S}_{j,k+1}(v^{\rm S}_{j,k+1})^2+L^{\rm S}_{j,k+1}\right)}{b^+_{j,k+\frac12}-b^-_{j,k+\frac12}}$$
$$+\beta_{j,k+\frac12}\big((\rho v)^{\rm S}_{j,k+1}-(\rho v)^{\rm N}_{j,k}-\delta(\rho v)_{j,k+\frac12}\big),$$

$$\mathcal{G}^{(4)}_{j,k+\frac12}=\frac{b^+_{j,k+\frac12}v^{\rm N}_{j,k}(E^{\rm N}_{j,k}+(\rho\phi)^{\rm N}_{j,k}+p^{\rm N}_{j,k})-b^-_{j,k+\frac12}v^{\rm S}_{j,k+1}(E^{\rm S}_{j,k+1}+(\rho\phi)^{\rm S}_{j,k+1}+p^{\rm S}_{j,k+1})}{b^+_{j,k+\frac12}-b^-_{j,k+\frac12}}$$
$$+\beta_{j,k+\frac12}\big(E^{\rm S}_{j,k+1}-E^{\rm N}_{j,k}+H(\psi_{j,k+\frac12})\cdot\big((\rho\phi)^{\rm S}_{j,k+1}-(\rho\phi)^{\rm N}_{j,k}-\delta(E+\rho\phi)_{j,k+\frac12}\big),$$

where $(\rho\phi)^{\rm E}_{j,k}=\rho^{\rm E}_{j,k}\phi(x_{j+\frac12},y_k)$, $(\rho\phi)^{\rm W}_{j,k}=\rho^{\rm W}_{j,k}\phi(x_{j-\frac12},y_k)$, $(\rho\phi)^{\rm N}_{j,k}=\rho^{\rm N}_{j,k}\phi(x_j,y_{k+\frac12})$, $(\rho\phi)^{\rm S}_{j,k}=\rho^{\rm S}_{j,k}\phi(x_j,y_{k-\frac12})$, $\psi_{j,k+\frac12}=\frac{|K_{j+1,k}-K_{j,k}|}{\Delta x}\cdot\frac{x_{k_{r}+\frac12}-x_{k_{\ell}-\frac12}}{\max_{j,k}\{K_{j,k},K_{j+1,k}\}}$, $\psi_{j+\frac12,k}=\frac{|L_{j,k+1}-L_{j,k}|}{\Delta y}\cdot\frac{y_{k_{r}+\frac12}-y_{k_{\ell}-\frac12}}{\max_{j,k}\{L_{j,k},L_{j,k+1}\}}$, the function H is defined, as before, in (2.16), and

$$\delta\boldsymbol{q}_{j+\frac12,k}=\text{minmod}\big(\boldsymbol{q}^{\rm W}_{j+1,k}-\boldsymbol{q}^{*}_{j+\frac12,k},\,\boldsymbol{q}^{*}_{j+\frac12,k}-\boldsymbol{q}^{\rm E}_{j,k}\big)\tag{3.5}$$

and

$$\delta\boldsymbol{q}_{j,k+\frac12}=\text{minmod}\big(\boldsymbol{q}^{\rm S}_{j,k+1}-\boldsymbol{q}^{*}_{j,k+\frac12},\,\boldsymbol{q}^{*}_{j,k+\frac12}-\boldsymbol{q}^{\rm N}_{j,k}\big)\tag{3.6}$$

are build-in anti-diffusion terms with

$$\boldsymbol{q}^{*}_{j+\frac12,k}=\frac{a^+_{j+\frac12,k}\boldsymbol{q}^{\rm W}_{j+1,k}-a^-_{j+\frac12,k}\boldsymbol{q}^{\rm E}_{j,k}-\big\{\boldsymbol{F}(\boldsymbol{q}^{\rm W}_{j+1,k})-\boldsymbol{F}(\boldsymbol{q}^{\rm E}_{j,k})\big\}}{a^+_{j+\frac12,k}-a^-_{j+\frac12,k}}$$

and

$$\boldsymbol{q}^{*}_{j,k+\frac12}=\frac{b^+_{j,k+\frac12}\boldsymbol{q}^{\rm S}_{j,k+1}-b^-_{j,k+\frac12}\boldsymbol{q}^{\rm N}_{j,k}-\big\{\boldsymbol{G}(\boldsymbol{q}^{\rm S}_{j,k+1})-\boldsymbol{G}(\boldsymbol{q}^{\rm N}_{j,k})\big\}}{b^+_{j,k+\frac12}-b^-_{j,k+\frac12}}.$$

Notice that the anti-diffusion terms (3.5) and (3.6) can be rigorously derived from the fully discrete CU framework along the lines of (though slightly different from) [14]. Namely, while $\delta\boldsymbol{q}_{j+\frac12,k}$ and $\delta\boldsymbol{q}_{j,k+\frac12}$ in [14] are obtained by computing the slopes in the piecewise linear interpolant over the "side" domains $D_{j+\frac12,k}$ and $D_{j,k+\frac12}$ using the point values at their corners, here the corresponding terms are obtained from the same interpolants using the values at the midpoints of the long sides of the rectangles $D_{j+\frac12,k}$ and $D_{j,k+\frac12}$.

We can now state the following well-balanced property of the proposed 2-D CU scheme, whose proof is similar to that of Theorem 2.1 and thus it is presented in Appendix A.

Theorem 3.1. *The 2-D semi-discrete CU scheme described above is well-balanced in the sense that it exactly preserves the steady state (1.5).*

4. Numerical examples

In this section, we present a number of 1-D and 2-D numerical examples, in which we demonstrate the performance of the proposed well-balanced semi-discrete CU scheme.

In all of the examples below, we have used the three-stage third-order strong stability preserving (SSP) Runge–Kutta method (see, e.g., [8,9,28]) to solve the ODE systems (2.5) and (3.4). The CFL number has been set to 0.4. Also, we have used the following constant values: the minmod parameter $\theta = 1.3$ and the specific heat ratio $\gamma = 1.4$.

In Examples 2–4, the initial data correspond to the 1-D and 2-D steady-state solutions and their small perturbations. The designed well-balanced CU schemes are capable of exactly preserving discrete versions of the 1-D and 2-D steady states (2.4) and (1.5), respectively. In Appendix B, we provide a detailed description of how to construct such steady states.

4.1. One-dimensional examples

In all of the 1-D numerical experiments, we use a uniform mesh with the total number of grid cells $N = k_r - k_\ell + 1$.

Example 1—shock tube problem. The first example is a modification of the Sod shock tube problem taken from [23,32]. We solve the system (2.1)–(2.3) with $\phi(y) = y$ in the computational domain $[0, 1]$ using the following initial data:

$$(\rho(y,0), v(y,0), p(y,0)) = \begin{cases} (1,0,1), & \text{if } y \le 0.5,\\ (0.125,0,0.1), & \text{if } y > 0.5, \end{cases}$$

and reflecting boundary conditions at both ends of the computational domain. These boundary conditions are implemented using the ghost cell technique as follows:

$$\begin{aligned} &\overline{\rho}_{k_\ell-1} := \overline{\rho}_{k_\ell}, \quad v_{k_\ell-1} := -v_{k_\ell}, \quad L_{k_\ell-1} := L_{k_\ell},\\ &\overline{\rho}_{k_r+1} := \overline{\rho}_{k_r}, \quad v_{k_r+1} := -v_{k_r}, \quad L_{k_r+1} := L_{k_r}. \end{aligned}$$

We compute the solution using $N = 100$ uniformly placed grid cells and compare it with the reference solution obtained using $N = 2000$ uniform cells. In Fig. 4.1, we plot both the coarse and fine grid solutions at time $T = 0.2$. As one can see, the proposed CU scheme captures the solutions on coarse mesh quite well showing a good agreement with both the reference solution and the results obtained in [23,32].

Notice that the coarse mesh solution features some oscillations in the vicinity of the shock. These oscillations, however, seem to be the so-called "WENO-type oscillations" as they disappear when the mesh is refined.

Example 2—isothermal equilibrium solution. In the second example, taken from [32] (see also [20,23,30]), we test the ability of the proposed CU scheme to accurately capture small perturbations of the steady state

$$\rho(y) = e^{-\phi(y)}, \quad v(y) \equiv 0, \quad p(y) = e^{-\phi(y)}, \tag{4.1}$$

of the system (2.1)–(2.3) with the linear gravitational potential $\phi(y) = y$ (in fact, we use a discrete version of this steady state with $L(y) \equiv 1$, obtained as described in Appendix B.1).

We take the computational domain $[0, 1]$ and use a zero-order extrapolation at the boundaries:

$$\begin{aligned} &\overline{\rho}_{k_\ell-1} := \overline{\rho}_{k_\ell} e^{\Delta y (\phi_y)_{k_\ell}}, \quad v_{k_\ell-1} := v_{k_\ell}, \quad L_{k_\ell-1} := L_{k_\ell},\\ &\overline{\rho}_{k_r+1} := \overline{\rho}_{k_r} e^{-\Delta y (\phi_y)_{k_r}}, \quad v_{k_r+1} := v_{k_r}, \quad L_{k_r+1} := L_{k_r}. \end{aligned}$$

Note that the boundary conditions on L can be recast in terms of p and ρ as

$$p_{k_\ell-1} = p_{k_\ell} + \Delta y\, \overline{\rho}_{k_\ell} (\phi_y)_{k_\ell}, \quad p_{k_r+1} = p_{k_r} - \Delta y\, \overline{\rho}_{k_r} (\phi_y)_{k_r}.$$

We first numerically verify that the proposed CU scheme is capable of exactly preserving the steady state (4.1). We use several uniform grids at time $T = 1$ and observe that the initial conditions are preserved within the machine accuracy, while the errors in the non-well-balanced computations are of the second order of accuracy as shown in Table 4.1.

Next, we introduce a small initial pressure perturbation and consider the system (2.1)–(2.3) subject to the following initial data:

$$\rho(y,0) = e^{-y}, \quad v(y,0) \equiv 0, \quad p(y,0) = e^{-y} + \eta e^{-100(y-0.5)^2},$$

where η is a small positive number. In the numerical experiments, we use larger ($\eta = 10^{-2}$) and smaller ($\eta = 10^{-6}$) perturbations.

We first apply the proposed well-balanced CU scheme to this problem and compute the solution at time $T = 0.25$. The obtained pressure perturbation ($p(y, 0.25) - e^{-y}$) computed using $N = 200$ and 2000 (reference solution) uniform grid cells are plotted in Fig. 4.2 for both $\eta = 10^{-2}$ and 10^{-6}. As one can see, the scheme accurately captures both small and

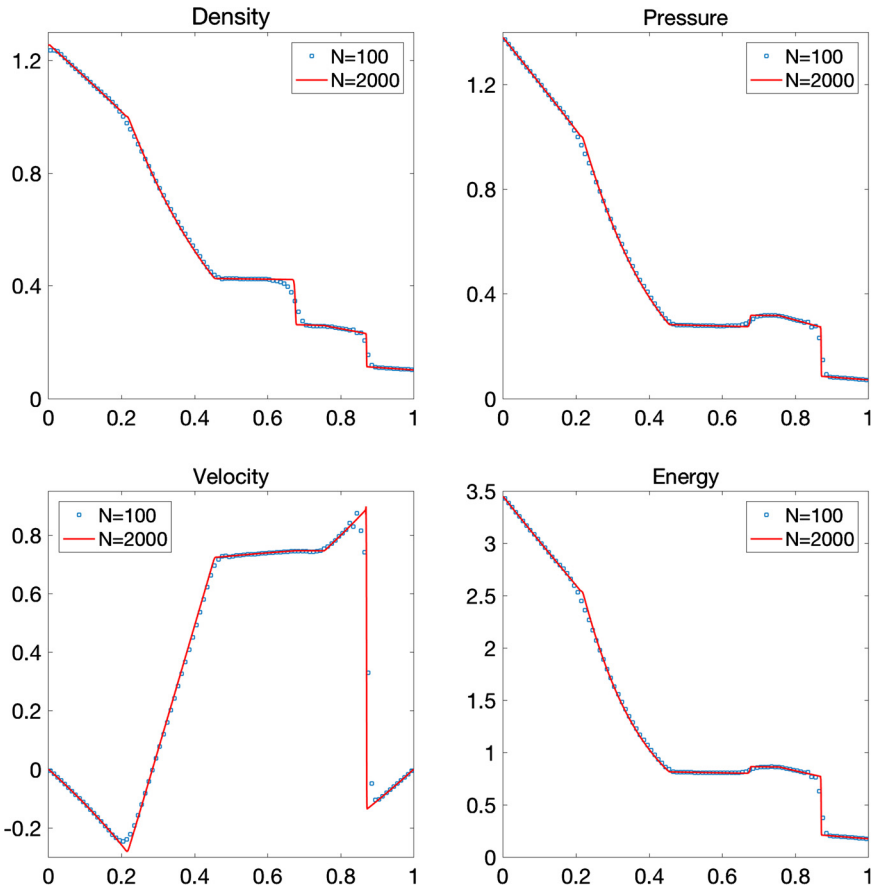

Fig. 4.1. Example 1: Solutions computed by the well-balanced CU scheme using $N = 100$ and 2000 cells.

Table 4.1
Example 2: L^1-errors and corresponding experimental convergence rates in the non-well-balanced computation of ρ, ρv and E; $\phi(y) = y$.

N	$\|\rho(\cdot,1) - \rho(\cdot,0)\|_1$	rate	$\|(\rho v)(\cdot,1) - (\rho v)(\cdot,0)\|_1$	rate	$\|E(\cdot,1) - E(\cdot,0)\|_1$	rate
100	1.47E-06	–	3.62E-06	–	4.25E-06	–
200	3.79E-07	1.95	9.07E-07	1.99	1.08E-06	1.99
400	9.62E-08	1.98	2.27E-07	1.99	2.72E-07	1.97
800	2.42E-08	1.99	5.69E-08	1.99	6.84E-08	1.99

large perturbations on a relatively coarse mesh with $N = 200$. In order to demonstrate the importance of the well-balanced property, we apply the non-well-balanced CU scheme described in the beginning of §2 to the same initial-boundary value problem (IBVP). The obtained results are shown in Fig. 4.2 as well. It should be observed that while the larger perturbation is quite accurately computed by both schemes, the non-well-balanced CU scheme fails to accurately capture the smaller one.

Finally, we test the experimental rate of convergence of the proposed well-balanced CU scheme by computing

$$\text{rate}_N := \log_2\left(\frac{||q_N^{(i)} - q_{2N}^{(i)}||_1}{||q_{2N}^{(i)} - q_{4N}^{(i)}||_1}\right), \quad i = 1, 2, 3,$$

where $q_N^{(i)}$ denotes the ith component of the solution computed using a uniform mesh with N cells. The obtained results, presented in Tables 4.2 and 4.3, demonstrate that the experimental rate of convergence is close to the expected second-order one for both $\eta = 10^{-2}$ and $\eta = 10^{-6}$.

Example 3—nonlinear gravitational potential. In this example, we consider the system (2.1)–(2.3) with the nonlinear gravitational potentials $\phi(y) = \frac{1}{2}y^2$ and $\phi(y) = \sin(2\pi y)$ subject to the steady-state initial data

$$\rho(y,0) = e^{-\phi(y)}, \quad v(y,0) \equiv 0, \quad p(y,0) = e^{-\phi(y)}, \tag{4.2}$$

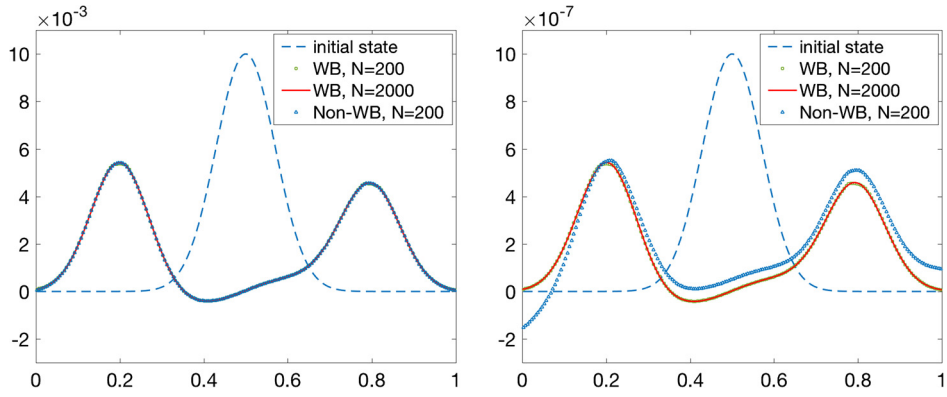

Fig. 4.2. Example 2: Pressure perturbation $(p(y,0.25)-e^{-y})$ computed by the well-balanced (WB) and non-well-balanced (Non-WB) CU schemes with $N=200$ and 2000 for $\eta=10^{-2}$ (left) and $\eta=10^{-6}$ (right).

Table 4.2
Example 2: L^1-errors and experimental convergence rates for the well-balanced CU scheme; $\eta=10^{-2}$.

N	$\|\rho_N-\rho_{2N}\|_1$	rate$_N$	$\|(\rho v)_N-(\rho v)_{2N}\|_1$	rate$_N$	$\|E_N-E_{2N}\|_1$	rate$_N$
100	2.04E-05	–	2.13E-05	–	7.67E-05	–
200	5.45E-06	1.90	5.20E-06	2.03	1.91E-05	2.00
400	1.33E-06	2.03	1.08E-06	2.25	4.13E-06	2.21
800	3.53E-07	1.91	2.36E-07	2.20	9.46E-07	2.12

Table 4.3
Example 2: Same as Table 4.2, but for $\eta=10^{-6}$.

N	$\|\rho_N-\rho_{2N}\|_1$	rate$_N$	$\|(\rho v)_N-(\rho v)_{2N}\|_1$	rate$_N$	$\|E_N-E_{2N}\|_1$	rate$_N$
100	3.53E-09	–	3.52E-09	–	2.43E-09	–
200	1.01E-09	1.80	8.53E-10	2.04	6.09E-10	1.99
400	1.91E-10	2.41	1.80E-10	2.24	1.28E-10	2.24
800	5.34E-11	1.84	3.86E-11	2.22	2.76E-11	2.21

(once again, we use discrete versions of these steady states with $L(y)\equiv 1$; see Appendix B.1) with the same boundary conditions as in Example 2. We first apply both the well-balanced and non-well-balanced CU schemes to this IBVP and compute the solution on a sequence of different meshes until the final time $T=1$. We observe that the while the well-balanced scheme preserves the steady state (4.2) within the machine accuracy, the errors in the non-well-balanced computations are of order of the scheme.

We, next, consider the same IBVP but with the following perturbed initial data:

$$\rho(y,0)=e^{-\phi(y)},\quad v(y,0)\equiv 0,\quad p(y,0)=e^{-\phi(y)}+\eta e^{-100(y-0.5)^2},\quad \eta=10^{-3}.$$

We compute the solution until the final time $T=0.25$ using both the well-balanced and non-well-balanced CU schemes. In Fig. 4.3 (left), we plot the pressure perturbations $(p(y,0.25)-e^{-\phi(y)})$ computed using the well-balanced scheme with $N=200$ and $N=2000$ (reference solution) uniform grid cells for $\phi(y)=\frac{1}{2}y^2$. For comparison, we plot the same perturbation computed by applying non-well-balanced CU scheme with $N=200$ uniform grid points. In Fig. 4.3 (right), we also include the results obtained by non-well-balanced CU scheme using a much finer mesh. One can conclude that only the well-balanced scheme can accurately capture the perturbation on a coarse grid, while a very fine mesh is required to control the perturbation with the non-well-balanced method.

In Fig. 4.4, we demonstrate the pressure perturbation $(p(y,0.25)-e^{-\phi(y)})$ obtained using both the well-balanced and non-well-balanced CU schemes on $N=200$ uniform grid cells for $\phi(y)=\sin(2\pi y)$. Similarly with the previous discussion, the proposed well-balanced CU scheme accurately resolves the perturbation on a coarse grid, while the non-well-balanced scheme requires much finer grid to capture the perturbation as accurately as the well-balanced method does.

4.2. Two-dimensional examples

In this section, we test the performance of the proposed well-balanced central-upwind scheme on two numerical examples and compare it with the performance of the corresponding non-well-balanced scheme. We note that the computational cost of the well-balanced scheme is in average about 25–40% higher than of its non-well-balanced counterpart when measured on the same grid. However, the resolution achieved by the well-balanced scheme is much higher. This is especially

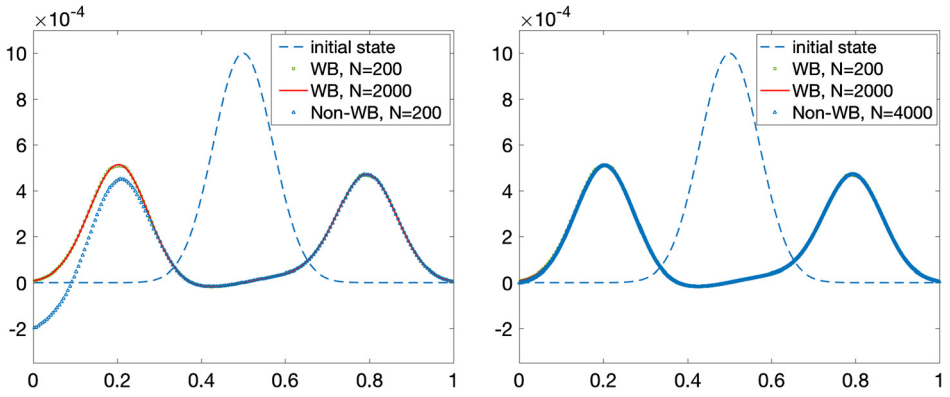

Fig. 4.3. Example 3: Pressure perturbation $(p(y, 0.25) - e^{-\phi(y)})$ computed by the well-balanced (WB) and non-well-balanced (Non-WB) CU schemes for $\phi(y) = \frac{1}{2}y^2$ with $N = 200$ for each scheme (left) and $N = 4000$ for the Non-WB scheme (right). The reference solution is computed using the WB scheme with $N = 2000$ grid points.

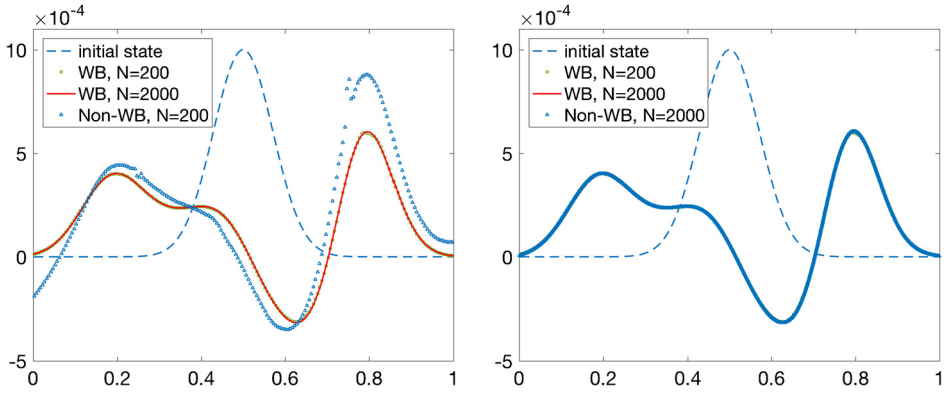

Fig. 4.4. Example 3: Pressure perturbation $(p(y, 0.25) - e^{-\phi(y)})$ computed by the well-balanced (WB) and non-well-balanced (Non-WB) CU schemes for $\phi(y) = \sin(2\pi y)$ with $N = 200$ for each scheme (left) and $N = 2000$ for the Non-WB scheme (right). The reference solution is computed using the WB scheme with $N = 2000$ grid points.

pronounced when course grd computations are conducted. In such cases, in order to achieve a comparable resolution by the non-well-balanced scheme, the computations must be performed on a much finer grid, which makes the non-well-balanced scheme significantly less efficient as demonstrated in Example 4.

Example 4—isothermal equilibrium solution. In the first 2-D example, which was introduced in [32], we consider the system (1.3) with $\phi(x, y) = x + y$ subject to the following initial data:

$$\rho(x, y, 0) = 1.21e^{-1.21\phi(x,y)}, \quad u(x, y, 0) \equiv v(x, y, 0) \equiv 0, \quad p(x, y, 0) = e^{-1.21\phi(x,y)}, \tag{4.3}$$

satisfying (1.5) and impose zero-order extensions at all of the four edges of the unit square $[0, 1] \times [0, 1]$. As in the 1-D case, we use a discrete version of (4.3) described in Appendix B.2 rather than its continuous counterpart (here, $L(x, y, 0) = e^{-1.21x}$ and $K(x, y, 0) = e^{-1.21y}$).

We first use the discrete steady-state data and verify that they are preserved within the machine accuracy, when the solution is computed by the proposed well-balanced CU scheme. On contrary, the non-well-balanced CU scheme preserves the initial equilibrium within the accuracy of the scheme only.

Next, we add a small perturbation to the initial pressure and replace $p(x, y, 0)$ in (4.3) with

$$p(x, y, 0) = e^{-1.21\phi(x,y)} + \eta e^{-121\left((x-0.3)^2+(y-0.3)^2\right)}, \quad \eta = 10^{-6}.$$

In Fig. 4.5 and the upper row of Fig. 4.6, we plot the pressure perturbation computed by both the well-balanced and non-well-balanced CU schemes at time $T = 0.15$ using 100×100 uniform cells. As one can clearly see, the well-balanced CU scheme can capture the perturbation accurately (and it takes only in 2.18 seconds on a laptop), while the non-well-balanced one produces spurious waves. When the mesh is refined to 800×800 uniform cells, the well-balanced solution remains oscillation-free; see Fig. 4.6 (lower left), and the spurious waves appearing in the non-well-balanced solution disappear; see Fig. 4.6 (lower right). We stress that the non-well-balanced 800×800 computation takes 1180.80 seconds on the same

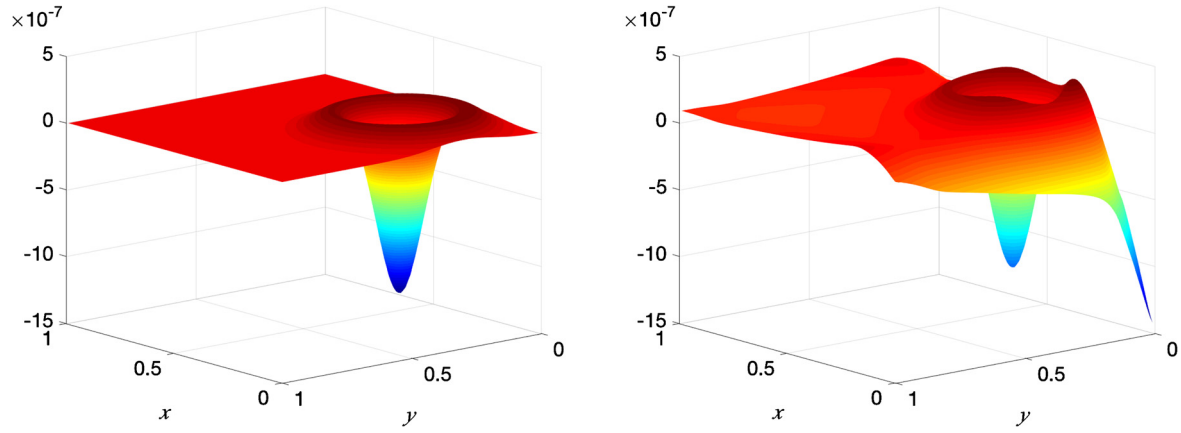

Fig. 4.5. Example 4: Pressure perturbation computed by the well-balanced (left) and non-well-balanced (right) CU schemes using 100×100 uniform cells.

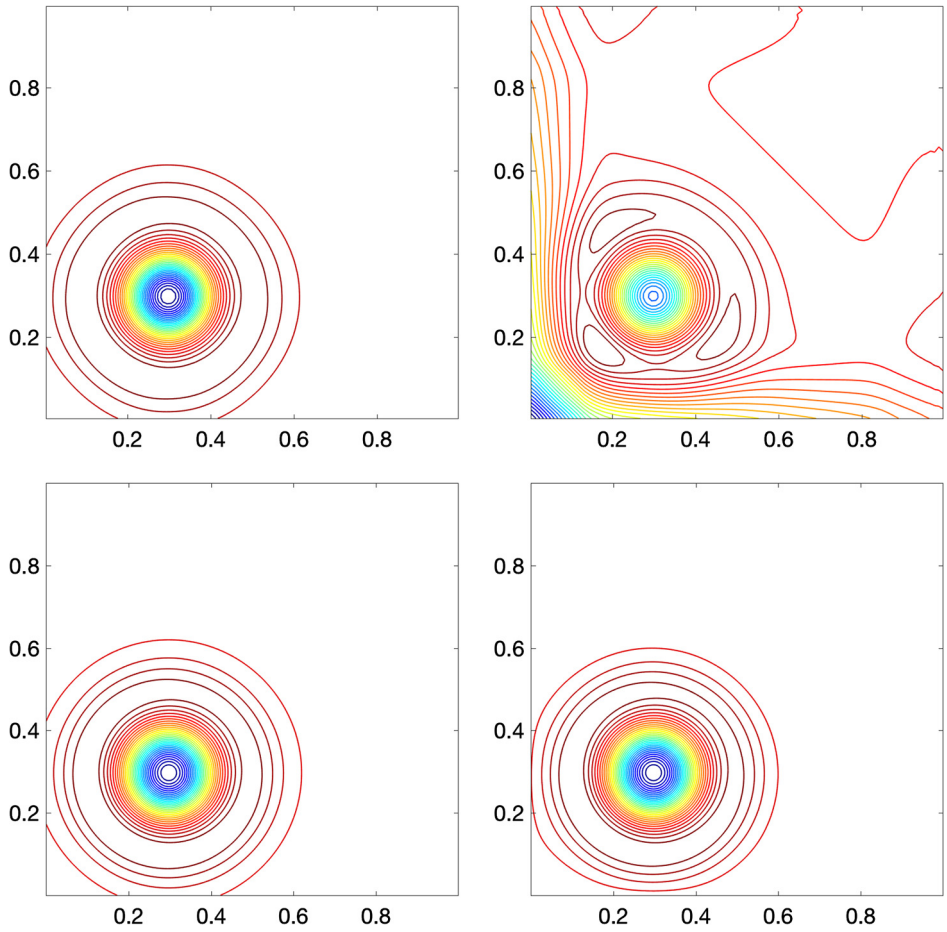

Fig. 4.6. Example 4: Contour plot of the pressure perturbation computed by well-balanced (left column) and non-well-balanced (right column) CU schemes using 100×100 (upper row) and 800×800 (lower row) uniform cells.

laptop. One can conclude that while the well-balanced CU scheme captures the perturbation efficiently on a coarse grid, the non-well-balanced CU scheme consumes very long time to achieve similar results.

Example 5—Explosion. In the second 2-D example, we compare the performance of well-balanced and non-well-balanced CU schemes in an explosion setting and demonstrate nonphysical shock waves generated by non-well-balanced scheme.

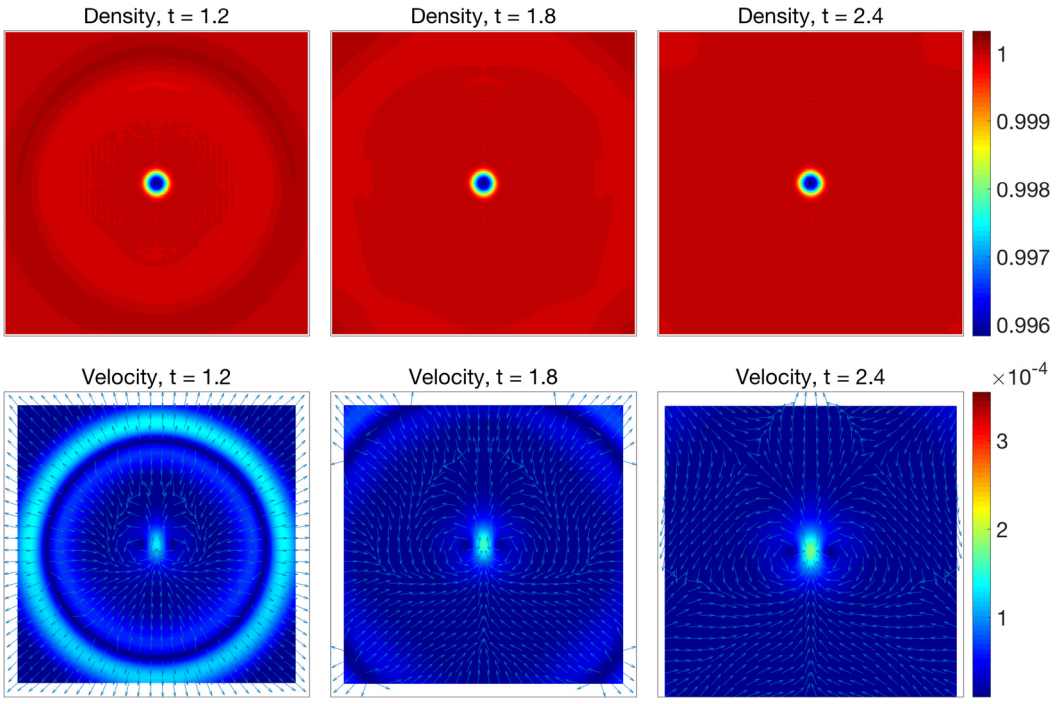

Fig. 4.7. Example 5: Density (ρ) and velocity ($\sqrt{u^2+v^2}$) computed by the well-balanced CU scheme in the domain $[0,3]\times[0,3]$.

We solve the system (1.3) with $\phi(x,y)=0.118y$ in the computational domain $[0,3]\times[0,3]$ subject to the following initial data:

$$\rho(x,y,0)\equiv 1,\quad u(x,y,0)\equiv v(x,y,0)\equiv 0,$$
$$p(x,y,0)=1-\phi(x,y)+\begin{cases}0.005, & (x-1.5)^2+(y-1.5)^2<0.01,\\ 0, & \text{otherwise.}\end{cases}$$

Zero-order extrapolation is used as the boundary conditions in all of the directions.

We use a uniform grid with 101×101 cells and compute the solution by both the well-balanced and non-well-balanced CU schemes until the final time $T=2.4$. At first, a circular shock wave is developed and later on it transmits through the boundary. Due to the heat generated by the explosion, the gas at the center expands and its density decreases generating a positive vertical momentum at the center of the domain. In Figs. 4.7 and 4.8, we plot the solution (ρ and $\sqrt{u^2+v^2}$ at times $t=1.2$, 1.8 and 2.4) computed by the well-balanced and non-well-balanced schemes, respectively. As one can see, the well-balanced scheme accurately captures the behavior of the solution at all stages, while the non-well-balanced scheme produces significant oscillations at the smaller time $t=1.2$, which starts dominating the solution, especially its velocity field, by the final time $T=2.4$.

5. Conclusion

We have presented a new well-balanced CU scheme for the Euler equations with gravitation. Our scheme is based on a new conservative reformulation of the original system of balance laws. This reformulation is obtained by introducing new global equilibrium variables which are also used in the reconstruction step and together with a well-balanced time evolution ensure the well-balanced property of the resulting numerical method.

It should be observed that in some astrophysical applications the gravitational energy $\rho\phi$ may be orders of magnitude larger than the fluid energy E. We have not considered such cases in the current paper, but would like to point out that combining relatively small fluid dynamics quantities p and E with larger gravitational quantities Q, R and $\rho\phi$, may, in principle, lead to inaccurate calculations of point values of p and E from the reconstructed values of new variables $K=p+Q$, $L=p+R$ and $E+\rho\phi$. The applicability of the proposed well-balanced approach in these special cases should be studied separately.

We would also like to note that in the studied system (1.2) and its 1-D version the gravitational potential ϕ is assumed to be time-independent. In the case of time-dependent ϕ the conservative reformulations (1.3), (1.4) and (2.1), (2.2) are not valid. However, one can still introduce the global fluxes in the momenta equations, while treating the source term in the energy equation using the midpoint quadrature, which will lead to a well-balanced central-upwind scheme.

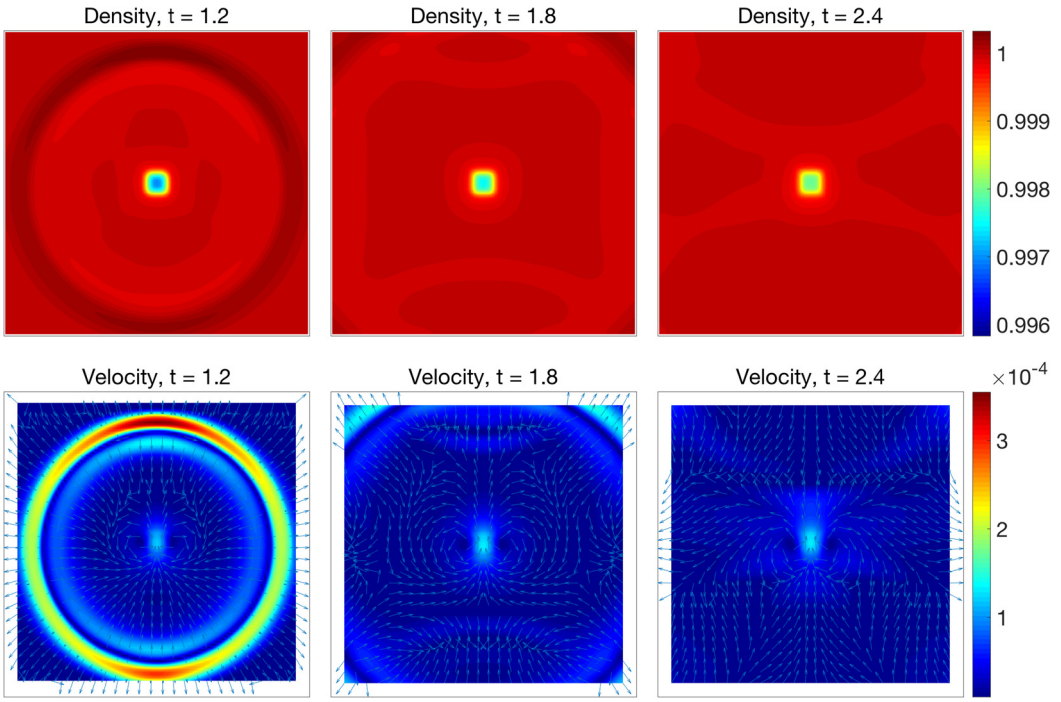

Fig. 4.8. Example 5: Density (ρ) and velocity ($\sqrt{u^2+v^2}$) computed by the non-well-balanced CU scheme in the domain $[0,3]\times[0,3]$.

Acknowledgements

The work of A. Chertock was supported in part by NSF grant DMS-1521051. The work of A. Kurganov was supported in part by NSF grant DMS-1521009 and NSFC grant 11771201. The work of Ş. N. Özcan was supported in part by the Turkish Ministry of National Education. The work of E. Tadmor was supported in part by ONR grant N00014-1512094 and NSF grants RNMS11-07444 (Ki-Net) and DMS-1613911.

Appendix A. Proof of Theorem 3.1

Assume that at certain time level, we have

$$u^{\mathrm{E}}_{j,k}=u^{\mathrm{W}}_{j,k}=u^{\mathrm{N}}_{j,k}=u^{\mathrm{S}}_{j,k}=v^{\mathrm{E}}_{j,k}=v^{\mathrm{W}}_{j,k}=v^{\mathrm{N}}_{j,k}=v^{\mathrm{S}}_{j,k}\equiv 0 \tag{A.1}$$

and

$$K^{\mathrm{E}}_{j,k}=K^{\mathrm{W}}_{j,k}=\widehat{K}_k,\ \ \forall j,\qquad L^{\mathrm{N}}_{j,k}=L^{\mathrm{S}}_{j,k}=\widehat{L}_j,\ \ \forall k, \tag{A.2}$$

where $\widehat{K}_k$ and $\widehat{L}_j$ only depend on k and j, respectively. In order to prove that the proposed scheme is well-balanced, we will show that for the data in (A.1) and (A.2) the x-numerical fluxes $\mathcal{F}_{j+\frac12,k}$ depend on k only, while the y-numerical fluxes $\mathcal{G}_{j,k+\frac12}$ depend on j only. This will ensure that the RHS of (3.4) is identically equal to zero at such steady states.

Indeed, the first components of the numerical fluxes, $\mathcal{F}^{(1)}_{j+\frac12,k}$ and $\mathcal{G}^{(1)}_{j,k+\frac12}$, vanish since (A.1) is satisfied and (A.2) implies $H(\psi_{j+\frac12,k})=H(\psi_{j,k+\frac12})=H(0)=0$. The second component of the x-numerical flux is $\mathcal{F}^{(2)}_{j+\frac12,k}=\widehat{K}_k$ since $u^{\mathrm{E}}_{j,k}=u^{\mathrm{W}}_{j+1,k}=0$ and $K^{\mathrm{E}}_{j,k}=K^{\mathrm{W}}_{j+1,k}=\widehat{K}_k$. Similarly, the third component of the y-numerical flux is $\mathcal{G}^{(3)}_{j,k+\frac12}=\widehat{L}_j$ since $v^{\mathrm{N}}_{j,k}=u^{\mathrm{S}}_{j,k+1}=0$ and $L^{\mathrm{N}}_{j,k}=L^{\mathrm{S}}_{j,k+1}=\widehat{L}_j$. Next, (A.1) implies that the third component of the x-numerical flux and the second component of the y-numerical flux, $\mathcal{F}^{(3)}_{j+\frac12,k}$ and $\mathcal{G}^{(2)}_{j,k+\frac12}$, vanish. Finally, the fourth component of the x-numerical flux vanishes:

$$\begin{aligned}\mathcal{F}^{(4)}_{j+\frac12,k}&=\alpha_{j+\frac12,k}\Big[E^{\mathrm{W}}_{j+1,k}-E^{\mathrm{E}}_{j,k}+H(\psi_{j+\frac12,k})\cdot\Big((\rho\phi)^{\mathrm{W}}_{j+1,k}-(\rho\phi)^{\mathrm{E}}_{j,k}-\delta(E+\rho\phi)_{j+\frac12,k}\Big)\Big]\\&=\frac{\alpha_{j+\frac12,k}}{\gamma-1}\cdot\frac{p^{\mathrm{W}}_{j+1,k}-p^{\mathrm{E}}_{j,k}}{2}=\frac{\alpha_{j+\frac12,k}}{2(\gamma-1)}\Big[\big(K^{\mathrm{W}}_{j+1,k}-Q_{j+\frac12,k}\big)-\big(K^{\mathrm{E}}_{j,k}-Q_{j+\frac12,k}\big)\Big]=0,\end{aligned}$$

since $K^{\mathrm{E}}_{j,k} = K^{\mathrm{W}}_{j+1,k} = \widehat{K}_k$ for all j. Similarly, the fourth component of the y-numerical flux also vanishes:

$$\begin{aligned}\mathcal{G}^{(4)}_{j,k+\frac{1}{2}} &= \beta_{j,k+\frac{1}{2}}\left[E^{\mathrm{S}}_{j,k+1} - E^{\mathrm{N}}_{j,k} + H(\psi_{j,k+\frac{1}{2}})\cdot\left((\rho\phi)^{\mathrm{S}}_{j,k+1} - (\rho\phi)^{\mathrm{N}}_{j,k} - \delta(E+\rho\phi)_{j,k+\frac{1}{2}}\right)\right]\\ &= \frac{\beta_{j,k+\frac{1}{2}}}{\gamma-1}\cdot\frac{p^{\mathrm{S}}_{j,k+1} - p^{\mathrm{N}}_{j,k}}{2} = \frac{\beta_{j,k+\frac{1}{2}}}{2(\gamma-1)}\left[\left(L^{\mathrm{S}}_{j,k+1} - R_{j,k+\frac{1}{2}}\right) - \left(L^{\mathrm{N}}_{j,k} - R_{j,k+\frac{1}{2}}\right)\right] = 0,\end{aligned}$$

since $L^{\mathrm{N}}_{j,k} = L^{\mathrm{S}}_{j,k+1} = \widehat{L}_j$ for all k. □

Appendix B. Discrete steady states

In this section, we describe a possible way discrete steady states can be constructed in both the 1-D and 2-D cases.

B.1. One-dimensional discrete steady states

The initial data corresponding to a 1-D discrete steady state can be constructed as follows. Given $\rho_k := \rho(y_k)$, $v_k := 0$, $L_k = L(y_k) = \text{Const}$, $k = k_\ell, \ldots, k_r$, we use the recursive formula (2.12) to obtain the discrete values R_k. Then, p_k are computed from (2.13), $p_k = L_k - R_k$, $k = k_\ell, \ldots, k_r$, and E_k are obtained from the EOS, $E_k = \frac{p_k}{\gamma-1} + \frac{1}{2}\rho_k(v_k)^2$, $k = k_\ell, \ldots, k_r$.

B.2. Two-dimensional discrete steady states

The initial data corresponding to a 2-D discrete steady state can be constructed in a similar though more complicated way. In the 2-D case, both $u_{j,k} = v_{j,k} = 0$, but neither L nor K are constant throughout the computational domain. However, since L is independent of y and K is independent of x, we have $L_{j,k} = L_j$ and $K_{j,k} = K_k$, $j = j_\ell, \ldots, j_r$, $k = k_\ell, \ldots, k_r$, which are assumed to be given.

We now show how one can construct a steady-state solution for a specific case of $\phi(x,y) = \phi(x+y)$, which is satisfied by ϕ used in Example 4.

We first set the zero values of Q and R (introduced in (1.4)) at the right and bottom parts of the boundary, respectively (alternatively, one could set the zero values of R and S at the left and upper parts):

$$Q_{j_r+\frac{1}{2},k} = 0, \quad k = k_\ell, \ldots, k_r, \qquad R_{j,k_\ell-\frac{1}{2}} = 0, \quad j = j_\ell, \ldots, j_r.$$

We then obtain the discrete values of $\rho_{j,k}$ and $p_{j,k}$ recursively as $j = j_r, \ldots, j_\ell$ and $k = k_\ell, \ldots, k_r$:

$$\begin{aligned}\rho_{j,k} &= \frac{L_j - K_k - R_{j,k-\frac{1}{2}} + Q_{j+\frac{1}{2},k}}{\frac{\Delta x}{2}\phi_x + \frac{\Delta y}{2}\phi_y},\\ p_{j,k} &= \frac{L_j + K_k - R_{j,k-\frac{1}{2}} - Q_{j+\frac{1}{2},k} + \left(\frac{\Delta x}{2}\phi_x - \frac{\Delta y}{2}\phi_y\right)\rho_{j,k}}{2},\\ E_{j,k} &= \frac{p_{j,k}}{\gamma-1} + \frac{\rho_{j,k}}{2}(u^2_{j,k} + v^2_{j,k}),\\ Q_{j-\frac{1}{2},k} &= Q_{j+\frac{1}{2},k} - \Delta x\,\rho_{j,k}(\phi_x)_{j,k}, \qquad R_{j,k+\frac{1}{2}} = R_{j,k-\frac{1}{2}} + \Delta y\,\rho_{j,k}(\phi_y)_{j,k}.\end{aligned}$$

References

[1] E. Audusse, F. Bouchut, M.-O. Bristeau, R. Klein, B. Perthame, A fast and stable well-balanced scheme with hydrostatic reconstruction for shallow water flows, SIAM J. Sci. Comput. 25 (2004) 2050–2065.

[2] N. Botta, R. Klein, S. Langenberg, S. Lützenkirchen, Well-balanced finite volume methods for nearly hydrostatic flows, J. Comput. Phys. 196 (2004) 539–565.

[3] P. Chandrashekar, C. Klingenberg, A second order well-balanced finite volume scheme for Euler equations with gravity, SIAM J. Sci. Comput. 37 (2015) B382–B402.

[4] A. Chertock, M. Dudzinski, A. Kurganov, M. Lukáčová-Medviďová, Well-balanced schemes for the shallow water equations with Coriolis forces, Numer. Math. (2017), https://doi.org/10.1007/s00211-017-0928-0, in press.

[5] V. Desveaux, M. Zenk, C. Berthon, C. Klingenberg, A well-balanced scheme to capture non-explicit steady states in the Euler equations with gravity, Int. J. Numer. Methods Fluids 81 (2016) 104–127.

[6] U.S. Fjordholm, S. Mishra, E. Tadmor, Well-balanced and energy stable schemes for the shallow water equations with discontinuous topography, J. Comput. Phys. 230 (2011) 5587–5609.

[7] J.M. Gallardo, C. Parés, M. Castro, On a well-balanced high-order finite volume scheme for shallow water equations with topography and dry areas, J. Comput. Phys. 227 (2007) 574–601.

[8] S. Gottlieb, D.I. Ketcheson, C.-W. Shu, Strong Stability Preserving Runge–Kutta and Multistep Time Discretizations, World Scientific Publishing Co. Pte. Ltd., Hackensack, NJ, 2011.

[9] S. Gottlieb, C.-W. Shu, E. Tadmor, Strong stability-preserving high-order time discretization methods, SIAM Rev. 43 (2001) 89–112.

[10] J.M. Greenberg, A.Y. Leroux, A well-balanced scheme for the numerical processing of source terms in hyperbolic equations, SIAM J. Numer. Anal. 33 (1996) 1–16.
[11] S. Jin, A steady-state capturing method for hyperbolic systems with geometrical source terms, M2AN Math. Model. Numer. Anal. 35 (2001) 631–645.
[12] R. Käppeli, S. Mishra, Well-balanced schemes for the Euler equations with gravitation, J. Comput. Phys. 259 (2014) 199–219.
[13] R. Käppeli, S. Mishra, A well-balanced finite volume scheme for the Euler equations with gravitation the exact preservation of hydrostatic equilibrium with arbitrary entropy stratification, Astron. Astrophys. 587 (2016) A94.
[14] A. Kurganov, C.-T. Lin, On the reduction of numerical dissipation in central-upwind schemes, Commun. Comput. Phys. 2 (2007) 141–163.
[15] A. Kurganov, S. Noelle, G. Petrova, Semi-discrete central-upwind scheme for hyperbolic conservation laws and Hamilton–Jacobi equations, SIAM J. Sci. Comput. 23 (2001) 707–740.
[16] A. Kurganov, G. Petrova, A second-order well-balanced positivity preserving central-upwind scheme for the Saint-Venant system, Commun. Math. Sci. 5 (2007) 133–160.
[17] A. Kurganov, E. Tadmor, New high resolution central schemes for nonlinear conservation laws and convection–diffusion equations, J. Comput. Phys. 160 (2000) 241–282.
[18] A. Kurganov, E. Tadmor, Solution of two-dimensional Riemann problems for gas dynamics without Riemann problem solvers, Numer. Methods Partial Differ. Equ. 18 (2002) 584–608.
[19] R. LeVeque, Balancing source terms and flux gradients in high-resolution Godunov methods: The quasi-steady wave-propagation algorithm, J. Comput. Phys. 146 (1998) 346–365.
[20] R. LeVeque, D. Bale, Wave propagation methods for conservation laws with source terms, Int. Ser. Numer. Math. 130 (1999) 609–618.
[21] G. Li, Y. Xing, High order finite volume WENO schemes for the Euler equations under gravitational fields, J. Comput. Phys. 316 (2016) 145–163.
[22] K.-A. Lie, S. Noelle, On the artificial compression method for second-order nonoscillatory central difference schemes for systems of conservation laws, SIAM J. Sci. Comput. 24 (2003) 1157–1174.
[23] J. Luo, K. Xu, N. Liu, A well-balanced symplecticity-preserving gas-kinetic scheme for hydrodynamic equations under gravitational field, SIAM J. Sci. Comput. 33 (2011) 2356–2381.
[24] H. Nessyahu, E. Tadmor, Nonoscillatory central differencing for hyperbolic conservation laws, J. Comput. Phys. 87 (1990) 408–463.
[25] S. Noelle, Y. Xing, C.-W. Shu, High-order well-balanced schemes, in: Numerical Methods for Balance Laws, in: Quad. Mat., vol. 24, Dept. Math., Seconda Univ. Napoli, Caserta, 2009, pp. 1–66.
[26] B. Perthame, C. Simeoni, A kinetic scheme for the Saint-Venant system with a source term, Calcolo 38 (2001) 201–231.
[27] M. Ricchiuto, A. Bollermann, Stabilized residual distribution for shallow water simulations, J. Comput. Phys. 228 (2009) 1071–1115.
[28] C.-W. Shu, S. Osher, Efficient implementation of essentially non-oscillatory shock-capturing schemes, J. Comput. Phys. 77 (1988) 439–471.
[29] P. Sweby, High resolution schemes using flux limiters for hyperbolic conservation laws, SIAM J. Numer. Anal. 21 (1984) 995–1011.
[30] C.T. Tian, K. Xu, K.L. Chan, L.C. Deng, A three-dimensional multidimensional gas-kinetic scheme for the Navier-Stokes equations under gravitational fields, J. Comput. Phys. 226 (2007) 2003–2027.
[31] R. Touma, U. Koley, C. Klingenberg, Well-balanced unstaggered central schemes for the Euler equations with gravitation, SIAM J. Sci. Comput. 38 (2016) B773–B807.
[32] Y. Xing, C.-W. Shu, High order well-balanced WENO scheme for the gas dynamics equations under gravitational fields, J. Sci. Comput. 54 (2013) 645–662.
[33] Y. Xing, C.-W. Shu, S. Noelle, On the advantage of well-balanced schemes for moving-water equilibria of the shallow water equations, J. Sci. Comput. 48 (2011) 339–349.
[34] K. Xu, J. Luo, S. Chen, A well-balanced kinetic scheme for gas dynamic equations under gravitational field, Adv. Appl. Math. Mech. 2 (2010) 200–210.